Article

Neuron

TRIM46 Controls Neuronal Polarity and Axon Specification by Driving the Formation of Parallel Microtubule Arrays

Highlights

- TRIM46 specifically localizes to the proximal axon
- TRIM46 forms closely spaced, parallel microtubule fascicles
- TRIM46 is needed for uniform axonal microtubule orientation
- TRIM46 is required for axon specification and neuronal polarity in vitro and in vivo

Authors

Sam F.B. van Beuningen, Lena Will, Martin Harterink, ..., Lukas C. Kapitein, Esther de Graaff, Casper C. Hoogenraad

Correspondence

e.degraaff@uu.nl (E.d.G.), c.hoogenraad@uu.nl (C.C.H.)

In Brief

van Beuningen et al. show that tripartite motif-containing protein TRIM46 is localized to the proximal axon and forms closely spaced parallel microtubule arrays. Functional analysis demonstrates the importance of uniform axonal microtubule bundles for neuronal polarity and axon specification.

van Beuningen et al., 2015, Neuron *88*, 1208–1226
December 16, 2015
http://dx.doi.org/10.1016/j.neuron.2015.11.012

CellPress

CellPress

Neuron
Article

TRIM46 Controls Neuronal Polarity and Axon Specification by Driving the Formation of Parallel Microtubule Arrays

Sam F.B. van Beuningen,[1] Lena Will,[1] Martin Harterink,[1] Anaël Chazeau,[1] Eljo Y. van Battum,[2] Cátia P. Frias,[1] Mariella A.M. Franker,[1] Eugene A. Katrukha,[1] Riccardo Stucchi,[1,3] Karin Vocking,[1] Ana T. Antunes,[1] Lotte Slenders,[1] Sofia Doulkeridou,[1] Peter Sillevis Smitt,[4] A.F. Maarten Altelaar,[3] Jan A. Post,[1] Anna Akhmanova,[1] R. Jeroen Pasterkamp,[2] Lukas C. Kapitein,[1] Esther de Graaff,[1,*] and Casper C. Hoogenraad[1,*]

[1]Cell Biology, Faculty of Science, Utrecht University, 3584 CH Utrecht, the Netherlands

[2]Department of Translational Neuroscience, Brain Center Rudolf Magnus, University Medical Center Utrecht, 3584 CG Utrecht, the Netherlands

[3]Biomolecular Mass Spectrometry and Proteomics, Bijvoet Center for Biomolecular Research, Utrecht Institute for Pharmaceutical Sciences and The Netherlands Proteomics Centre, Utrecht University, 3584 CH Utrecht, the Netherlands

[4]Department of Neurology, Erasmus Medical Center, 3015 CE Rotterdam, the Netherlands

*Correspondence: e.degraaff@uu.nl (E.d.G.), c.hoogenraad@uu.nl (C.C.H.)

http://dx.doi.org/10.1016/j.neuron.2015.11.012

SUMMARY

Axon formation, the initial step in establishing neuronal polarity, critically depends on local microtubule reorganization and is characterized by the formation of parallel microtubule bundles. How uniform microtubule polarity is achieved during axonal development remains an outstanding question. Here, we show that the tripartite motif containing (TRIM) protein TRIM46 plays an instructive role in the initial polarization of neuronal cells. TRIM46 is specifically localized to the newly specified axon and, at later stages, partly overlaps with the axon initial segment (AIS). TRIM46 specifically forms closely spaced parallel microtubule bundles oriented with their plus-end out. Without TRIM46, all neurites have a dendrite-like mixed microtubule organization resulting in Tau missorting and altered cargo trafficking. By forming uniform microtubule bundles in the axon, TRIM46 is required for neuronal polarity and axon specification in vitro and in vivo. Thus, TRIM46 defines a unique axonal cytoskeletal compartment for regulating microtubule organization during neuronal development.

INTRODUCTION

Axons are long, slender projections of a nerve cell that typically carry the electrical impulses away from the neuron's cell body. These long cellular structures are generated during development and maintained during the lifetime of an organism. Both axon outgrowth and maintenance largely depend on the organization and dynamics of the microtubule (MT) cytoskeleton. MTs form the structural backbones of the axon, as well as the highways for axonal transport essential for the supply of newly synthesized proteins and lipids (Conde and Cáceres, 2009; Maday et al., 2014). Mutations in human genes encoding for tubulin and MT-associated proteins cause a range of axon abnormalities and several neurological and neurodegenerative diseases have been linked to defects in axon architecture and transport-related processes (Millecamps and Julien, 2013; Zempel and Mandelkow, 2014). Regulation of axonal MT dynamics has also emerged as a key factor in axonal regrowth potential after spinal cord injury (Baas and Ahmad, 2013; Bradke et al., 2012; Chisholm, 2013). These studies highlight the importance of MTs for the structure and function of axons and MT remodeling as critical mechanism during axon regeneration.

In mature neurons, MTs are found throughout the whole axon; they form dense bundles in the shaft and these bundles extend into the growth cone where they spread out into single MTs (Conde and Cáceres, 2009; Hoogenraad and Bradke, 2009). Axonal MTs have several unique features, such as the fascicles of microtubules in the proximal part of the axon, which are groups of closely spaced microtubules linked by thin cross-bridges (Leterrier and Dargent, 2014; Rasband, 2010). The microtubule fascicles are seen on transverse electron microscopy sections and are used as morphological criteria to identify the axon initial segment (AIS) (Palay et al., 1968; Peters et al., 1968). In contrast to dendrites, axonal MTs have a unique parallel organization (Baas and Lin, 2011). Axons contain linear arrays of uniformly polarized MTs with the minus-ends pointing toward the cell body and the plus-ends pointing outward to the distal tips. Electron microscopy and live cell imaging studies have shown that uniform plus-end out MTs in axons are a universal and evolutionarily conserved signature of axons (Baas and Lin, 2011; Conde and Cáceres, 2009; Hoogenraad and Bradke, 2009). Using both assays in organisms ranging from the invertebrate to mammals, >95% of axonal MTs have been found to be plus-end out (Baas et al., 1988; Kleele et al., 2014; Stepanova et al., 2003; Stone et al., 2008). The uniformly oriented axonal MTs probably drive polarized cargo transport (Kapitein and

Hoogenraad, 2011). It has been shown that MT plus-end-directed kinesin displays a higher affinity toward axonal MTs, which could promote the transport of specific cargos into the axon (Hammond et al., 2010; Kapitein et al., 2010; Nakata and Hirokawa, 2003). In contrast, little is known about how the unique uniform MT orientation is built up and maintained in axons.

MT-based mechanisms are not only important for regulating architecture and cargo trafficking in mature axons, they also have an instructive role in the polarization of neurons and establishment of axon identity (Conde and Cáceres, 2009; Hoogenraad and Bradke, 2009). The transition from a symmetric to an asymmetric cell shape begins when a single neurite initiates a phase of rapid growth to become the axon, while other cell extensions later differentiate into dendrites. This symmetry breaking is the initial step of neuronal polarization, which largely depends on cytoskeletal rearrangements (Barnes and Polleux, 2009; Conde and Cáceres, 2009). Several studies have demonstrated that MTs, in parallel with the actin cytoskeleton, determine the initial polarization of neurons (Conde and Cáceres, 2009; Hoogenraad and Bradke, 2009). Axon formation critically depends on local MT reorganization and is characterized by the formation of parallel MT bundles with their plus-ends pointing outward (Baas and Lin, 2011). It was also shown that MT stabilization in one of the undifferentiated neurites of hippocampal neurons is sufficient to break symmetry and specify axon formation (Witte et al., 2008). Therefore, stabilization and bundling of parallel MTs in the future axon could be key processes underlying neuronal polarization. This model also suggests that specific MT-associated proteins may localize to the newly specified axon and locally regulate uniform MT orientation. An important challenge is thus to identify factors that regulate neuronal polarization by setting up axon-specific MT organization.

In this study, we use a combination of immunohistochemical, biochemical, and cell-biological approaches, live cell imaging, quantitative/high-resolution microscopy, and in utero electroporation to determine the role of the newly identified MT-associated protein TRIM46, which belongs to the tripartite motif containing (TRIM) protein family. We show that TRIM46 specifically localizes to the newly specified axon and organizes uniform MT orientation in axons. Moreover, TRIM46 is required for axon specification and neuronal polarity in vitro and in vivo. We propose a model in which the formation of uniform MTs in the axonal shaft initiates the polarity of neurons.

RESULTS

Identification of TRIM46 as an Autoantigen in the Proximal Axon

Human autoimmune antibodies have helped to identify several new antigens, including antigens at the axon initial segment (Berghs et al., 2001; Notturno et al., 2014). Previous studies showed that two autoimmune antibodies display immunoreactivity with the proximal axon of Purkinje cells in cerebellum sections (Figures 1A and S1A) (Sabater et al., 2013; Shams'ili et al., 2009). We set out to identify the axon-specific antigen by performing immunoprecipitation experiments on crude rat brain extracts using the serum reported by Shams'ili et al., followed by mass spectrometry (Figures 1B and S1B). The results were compared to datasets obtained from previous mass spectrometry experiments (de Graaff et al., 2012), and we identified TRIM46 (tripartite motif family member 46), also named TRIFIC (tripartite, fibronectin type III, and C-terminal B30.2-like motif) (Short and Cox, 2006), as a unique protein pulled down by the autoimmune serum. TRIM46 is a member of the C-I TRIM family, a subfamily of the RBCC (N-terminal RING finger/B-box/coiled coil)/TRIM superfamily (Short and Cox, 2006). Many proteins containing a RING finger domain play a role in the ubiquitination pathway (Ikeda and Inoue, 2012; Short and Cox, 2006). However, ubiquitin E3 ligase activity and putative substrates for TRIM46 have not been reported and no interaction was found with ubiquitin-conjugating E2 enzymes (Deshaies and Joazeiro, 2009; Napolitano et al., 2011).

To confirm the presence of TRIM46-specific antibodies in the autoimmune sera, we performed immunoprecipitation experiments with extracts of HEK293 cells expressing GFP-tagged TRIM46. In contrast to control serum, both autoimmune sera pulled down GFP-TRIM46 and not control GFP (Figures 1C and S1C). We next performed cell-based assays to find further evidence for TRIM46 as the antigen that is recognized by the autoimmune antibodies. Both sera and a newly generated rabbit TRIM46 antibody strongly stained HeLa cells expressing GFP-TRIM46, but not the surrounding untransfected cells or control cells expressing the close homolog GFP-TRIM36 (Figures 1D, S1D, S1G, and S1H). Consistent with a previous report (Short and Cox, 2006), both TRIM46 and TRIM36 label the MT cytoskeleton in HeLa cells (Figure S1E). To determine whether TRIM46 is the autoantigen localized at the proximal axon, we next used RNAi to deplete endogenous TRIM46 in primary neuronal cultures and analyzed immunofluorescent staining patterns. The efficiency of TRIM46 protein depletion was first tested by introducing two independent TRIM46 shRNAs into cortical neurons. Western blot analysis revealed that both shRNAs reduced the levels of TRIM46 by ~80% (Figures 1E and 1F), which was also confirmed by comparative mass spectrometry (Figure S1F). Staining of differentiated hippocampal neurons at 5 days in vitro (DIV5) transfected with TRIM46 shRNAs with the autoimmune sera or the rabbit TRIM46 antibody confirmed that the TRIM46 staining at the proximal axon was reduced by ~80% compared to control cells. In neurons expressing both TRIM46 shRNAs, the axonal TRIM46 staining was reduced by ~90% (Figures 1G and 1H). Together, these results demonstrate that TRIM46 is the antigen in the proximal axon detected by the autoimmune antibodies.

TRIM46 Specifically Localizes to the Proximal Axon and Defines the Compartment between Somatodendritic MAP2 and Axonal Tau

To gain more insight into the role of TRIM46, we first analyzed the localization of TRIM46 in the nervous system. Immunofluorescence labeling of mouse brain sections showed that TRIM46 is specially enriched in the initial part of the axon, as outlined by the cerebellar Purkinje cell marker Calbindin (Figure S2A). The axonal TRIM46 staining pattern partly overlaps with Ankyrin-G (AnkG) staining, which outlines the axon initial segment (AIS) (Figures 2A and 2B). TRIM46 co-distributes with AnkG throughout the CNS and is present in the proximal axon of all

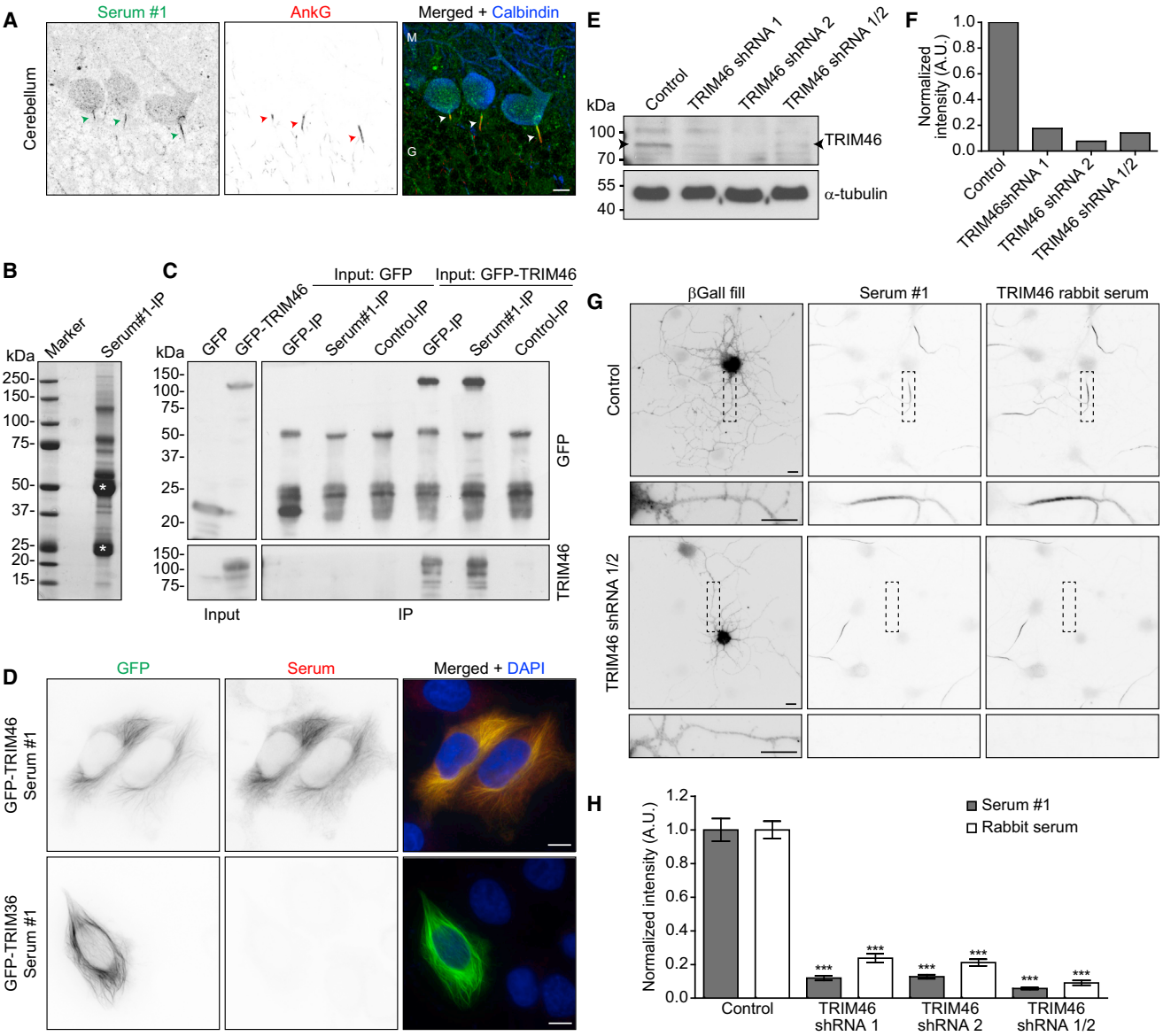

Figure 1. Identification of TRIM46 as an Autoimmune Antigen

(A) Mouse cerebellum sections stained with autoimmune serum #1 (green) together with AnkG (red) and Calbindin (blue). G, granular layer; M, molecular layer.

(B) Coomassie-stained gel of total rat brain extract immunoprecipitated with serum #1. IgG bands are indicated with a white asterisk.

(C) Western blot analysis of HEK293 cell extracts expressing GFP or GFP-TRIM46 and immunoprecipitated using anti-GFP antibodies, serum #1, or control serum.

(D) HeLa cells expressing either GFP-TRIM46 or GFP-TRIM36 (green) stained with serum #1 (red).

(E and F) Western blot analysis (E) and quantifications of cortical neurons (DIV7) (F) expressing indicated constructs. Arrowheads indicate TRIM46 band.

(G) Representative images of DIV5 hippocampal neurons co-transfected at DIV1 with β-galactosidase (blue) together with pSuper control or TRIM46-shRNA#1/2 and co-stained with serum #1 (green) and rabbit serum against TRIM46 (red).

(H) Quantification of the normalized intensities of serum #1 and TRIM46 rabbit serum stainings in neurons (DIV5) transfected at DIV1 with pSuper control (n = 29), TRIM46-shRNA#1 (n = 30), TRIM46-shRNA#2 (n = 30), or TRIM46-shRNA#1/2 (n = 30).

Error bars represent SEM. ***$p < 0.001$ comparing control versus individual conditions (t test). a.u., arbitrary units. Scale bar represents 10 μm in (A), (D), and (G).

neuronal types examined, including pyramidal neurons and interneurons in cortex and hippocampus and all neuronal cell types in the cerebral and cerebellar cortex (Figures 2A, 2B, and S2A–S2C). Interestingly, TRIM46 staining is also detected in the proximal axon of dorsal root ganglion (DRG) neurons in the peripheral nervous system (Figure S2D). In contrast to AnkG, TRIM46 is not detected at the nodes of Ranvier in the mouse sciatic nerve (Figure S2E).

To further analyze the subcellular distribution of TRIM46, we stained fully polarized hippocampal neurons in culture at DIV7.

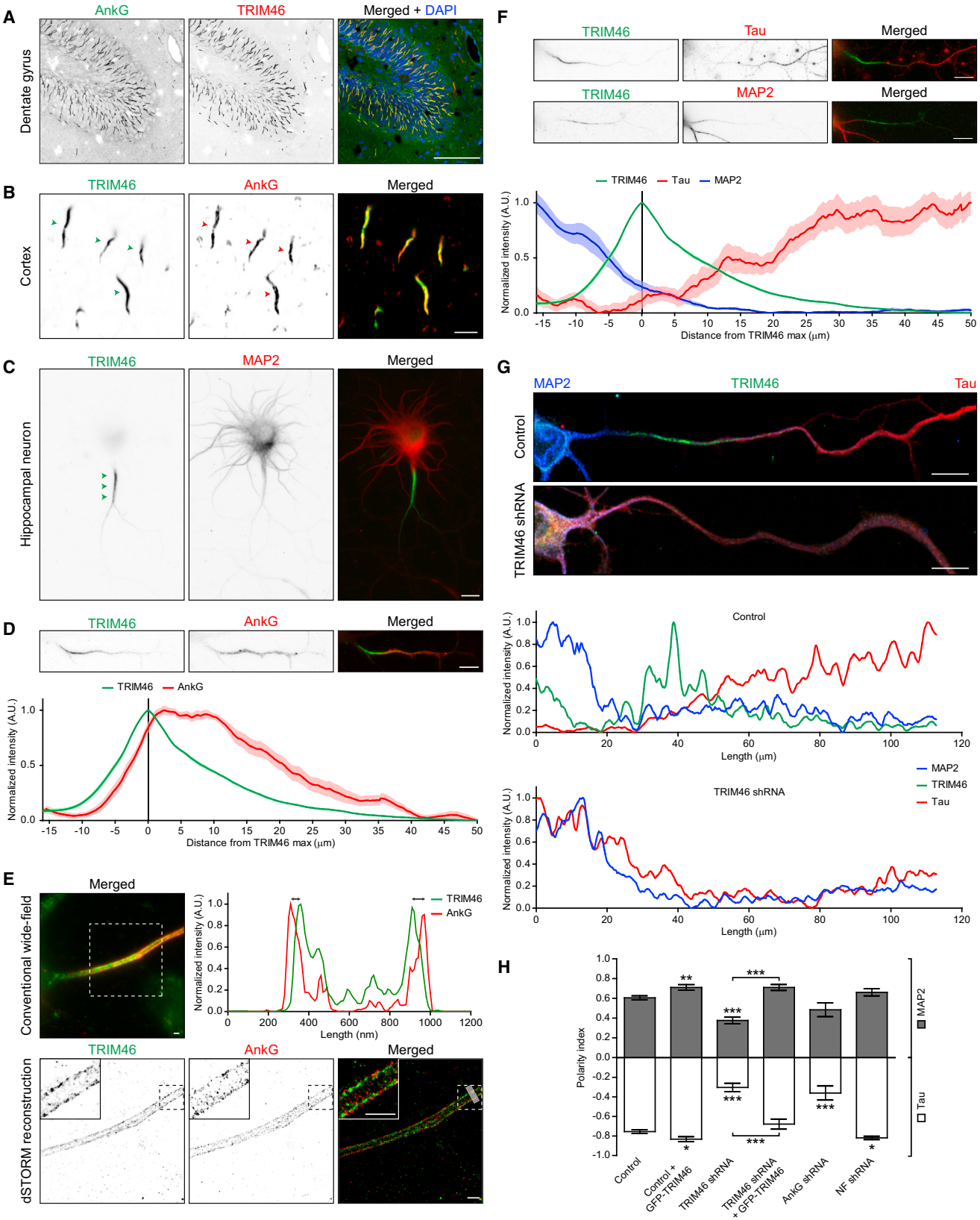

(legend on next page)

Consistent with the immunohistochemistry data, TRIM46 was absent from the cell body and dendrites but highly enriched in the initial part of the axon (Figure 2C). Similar results were obtained by immunostaining with the autoimmune serum (Figure 1G) and by low-level expression of GFP-TRIM46 in cultured neurons (Figure S3A). Interestingly, GFP-TRIM36 did not localize to the proximal axon (Figure S3A). The TRIM46 staining pattern overlapped with the more proximal region of the AIS (Figures 2D and S3B). However, direct stochastic optical reconstruction microscopy (dSTORM) imaging revealed that AnkG and TRIM46 mark two separate axonal domains. Quantification of the peak-to-peak distance revealed that AnkG coincides with βIV-spectrin at the axonal plasma membrane but is separated from the TRIM46 signal, which localizes more inside the axonal shaft at ~50 nm distance from AnkG (Figures 2E, S4A, and S4B). These data are consistent with pulldown experiments, where we could not detect an interaction between TRIM46 and AIS components (Figure S2F). We next determined the degree of co-localization with the somatodendritic marker MAP2 and axonal marker Tau (Figures 2F and S3C). Quantitative analysis revealed that TRIM46 defines the axonal region between MAP2 and Tau (Figure 2F). TRIM46 depletion in differentiated neurons resulted in the polarized distribution loss of MAP2 and Tau and led to an overlap of these markers in the proximal part of the axon (Figures 2G and 2H). Line scans along the proximal axon demonstrate MAP2 staining in the proximal axon, high levels of Tau near the cell body, and decreasing Tau immunoreactivity at more distal locations in TRIM46 knockdown cells (Figure 2G). Together, these results demonstrate that in more mature neurons, TRIM46 labels an axonal subdomain between the soma and the proximal edge of the AIS and defines the barrier between somatodendritic MAP2 and axonal tau.

TRIM46 Is Not Required for AIS Maintenance but Needed for Proper Axon Morphology

Given previous observations that loss of AnkG also alters the MAP2 and Tau distribution (Hedstrom et al., 2008; Sobotzik et al., 2009), we examined the effect of TRIM46 knockdown on the localization of several AIS markers, including AnkG, βIV-spectrin, neurofascin (NF)-186, and voltage-gated sodium (Nav) channels. Depletion of TRIM46 in already polarized neurons only partly affected the AIS (Figure S5A), suggesting that TRIM46 is not required for AIS maintenance. Interestingly, knockdown of AnkG caused a marked TRIM46 redistribution, while depletion of other AIS proteins did not affect TRIM46 localization (Figures S5B and S5C). These data and the observed loss in polarized distribution of MAP2 and Tau in AnkG knockdown (Figure 2H) suggest that AnkG maintains the TRIM46 compartment between MAP2 and Tau, which is consistent with the critical role of AnkG in maintaining general axo-dendritic polarity (Hedstrom et al., 2008; Sobotzik et al., 2009). We next examined the effect of TRIM46 knockdown on the outgrowth of axons in differentiated neurons. In neurons at DIV5 expressing TRIM46 shRNAs and β-galactosidase (β-gal; to highlight neuronal morphology), we observed a marked change in axon morphology (Figure S5D). Quantification revealed a decrease of total axon length, primary axon length, number of axon branches, and a decrease in mean length per axon branch compared to control neurons that can be rescued by expression of GFP-TRIM46 (Figures S5D and S5E). These data indicate that TRIM46 is not required for AIS maintenance but is needed for proper axon morphology when neurons are already polarized.

The RING Finger and COS Box Localize TRIM46 to the Axon

We next identified the domains responsible for the axonal localization of TRIM46. Like all members of the RBCC/TRIM superfamily, TRIM46 has an N-terminal RBCC domain containing a RING finger, a B-box 1/2, and a coiled-coil region. TRIM46 also has a unique C-terminal subgroup one signature (COS) box between the RBCC domain and the C-terminal FN3 and B30.2-like domain (Figure 3A). By analyzing TRIM46 deletion constructs, we found that the N-terminal RING finger domain of TRIM46 is required for localization to the proximal axon in TRIM46-depleted neurons (Figures 3A and S3D). Like all TRIM family members, the TRIM46 RING finger domain contains a conserved Cys3HisCys4 motif that is critical for proper folding of the RING finger and its potential E3 ubiquitin-protein ligase activity (Figure S1H) (Ikeda and Inoue, 2012). Interestingly, the unfolded RING finger mutant TRIM46 (GFP-TRIM46 RING mutant), in which the conserved cysteine and histidine residues are mutated (Huang et al., 2012; Schwamborn et al., 2009), still localizes to the proximal axon (Figures 3A and S3D). In addition, blocking SUMOylation and proteasome activity by respectively Ginkgolic acid and MG132 has no effect on TRIM46 localization to the proximal axon (Figure S5H). These results indicate that not

Figure 2. Localization of TRIM46 to the Proximal Part of the Axon

(A and B) Sections of mouse dentate gyrus (A) and cerebral cortex (B) stained for AnkG (green) and TRIM46 (red).

(C) Cultured hippocampal neuron (DIV7) stained for TRIM46 (green) and MAP2 (red).

(D) Zoom of the proximal axon in DIV7 hippocampal neurons stained for TRIM46 (green) and AnkG (red). Diagram shows the average normalized fluorescent intensity profiles of TRIM46 (n = 179) and AnkG (n = 16).

(E) Representative image and dSTORM reconstruction including linescan (500 nm width) of DIV5 hippocampal neurons stained for TRIM46 (green) and AnkG (red). Localization precision is 15.1 nm for TRIM46 and 10.5 nm for AnkG.

(F) Zoom of the proximal axon in DIV7 hippocampal neurons stained for TRIM46 (green), Tau (red), and MAP2 (blue). Diagram shows the average normalized fluorescent intensity profiles of TRIM46 (n = 179), Tau (n = 23), and MAP2 (n = 11).

(G) Representative images of DIV4 cortical neurons expressing pSuper control or TRIM46-shRNA#1/2, and co-stained with MAP2 (blue), TRIM46 (green), and Tau (red). Diagram shows the individual fluorescent intensity profiles from the soma into the axon.

(H) Polarity index of MAP2 and Tau in cortical neurons (DIV4) expressing pSuper control (n = 28), pSuper Control and GFP-TRIM46 (shRNA non-targetable) (n = 12), TRIM46-shRNA#1/2 (n = 28), TRIM46-shRNA#1/2 and GFP-TRIM46 (shRNA non-targetable) (n = 12), AnkG-shRNA (n = 12), or NF-shRNA (n = 12).

Error lines (D and E) and bars (H) represent SEM. ***$p < 0.001$ comparing (unless differently indicated) control versus individual conditions (Mann-Whitney U Test). a.u., arbitrary units. Scale bar represents 1 μm in (E), 10 μm in (B), (C), (D), (F), and (G), and 100 μm in (A).

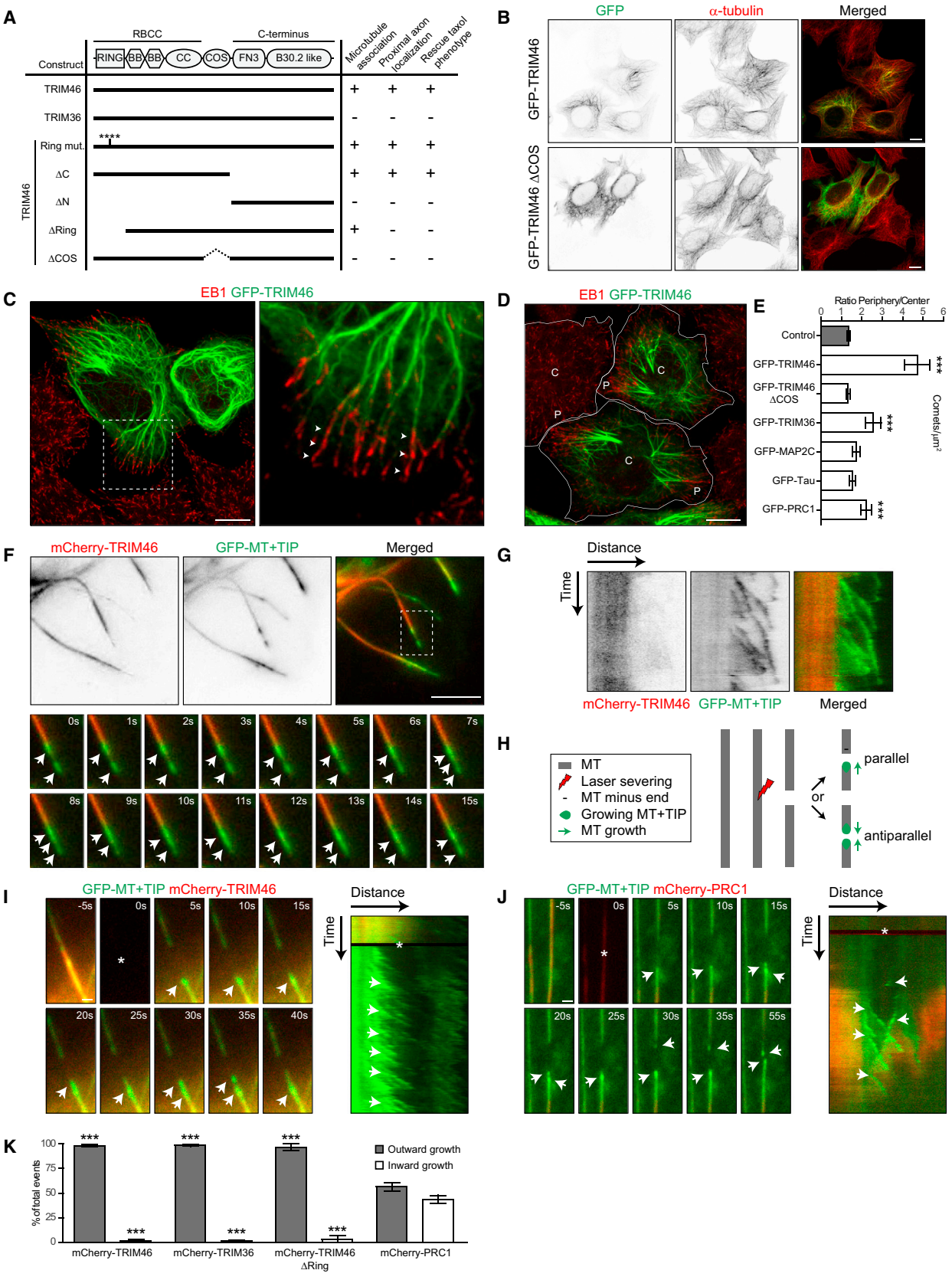

(legend on next page)

the folding and potential activity of the RING finger but the sequences within the RING domain contributes to the axonal localization of TRIM46.

Members of the C-I TRIM family, including TRIM46 and TRIM36, label the MT cytoskeleton in HeLa cells (Figure S1D). TRIM46 binds tubulin (Figure S2F) and previous analyses suggested that the coiled-coiled COS box is required for MT association (Short and Cox, 2006). Neurons treated with the MT depolymerizing drug nocodazole lost the specific TRIM46 staining (Figures S5F and S5G), indicating that association with MTs is required for the axonal localization of TRIM46. We then identified the region responsible for MT binding and found that the N-terminal region of TRIM46 (GFP-TRIM46 ΔC) is the minimal region required for MT association in HeLa cells (Figures 3A, 3B, S6A, and S6B). While the RING finger domain is not directly needed for MT binding, the COS box is needed to associate with MTs (Figures 3A, 3B, and S6). Like the N-terminal RING finger domain, the COS box is indispensable for localization to the proximal axon (Figures 3A and S3D). Together, these results suggest that both the N-terminal RING finger and MT binding properties of the COS box are collectively involved in the axon localization of TRIM46.

TRIM46 Forms Parallel Microtubule Arrays

We further examined the interaction between TRIM46 and MTs and its relevance for axonal MT organization. In contrast to GFP-MAP2C and GFP-Tau, GFP-TRIM46 expression in HeLa cells generated multiple MT bundles with the majority of their plus-ends pointing toward the cell periphery (Figures 3C–3E). Visualizing MT dynamics by using the plus-end marker GFP-MT+TIP showed that several comets grow from a single TRIM46-positive MT bundle (Figure 3F; Movie S1). When analyzed in more detail, we found that MT plus-end dynamics primarily occurs at the tips of the TRIM46 bundles (Figure 3G). Since MT bundles can be arranged in a parallel or in an antiparallel fashion, we studied the MT orientation in TRIM46 bundles using laser-based microsurgery (Yau et al., 2014). Cutting a MT bundle with a laser creates new MT ends and allows analysis of the newly generated MT plus-ends (Figure 3H). By observing the growth direction of GFP-MT+TIP comets after laser severing (LS), this assay permits a direct readout of MT orientation in a bundle. Upon LS of mCherry-TRIM46-positive MT bundles, the growth of newly formed GFP-MT+TIP comets is in one direction only (Figure 3I; Movie S2), similar to TRIM36 (Figure 3K). In contrast, expression of mCherry-PRC1, which is known to associate with anti-parallel MTs (Loïodice et al., 2005), allows MT growth recovery from two directions (Figure 3J; Movie S2). Quantification revealed that nearly all growth events within the TRIM46-positive bundles occurred in one direction, whereas the growth events are mixed in PRC1-labeled MTs (Figure 3K). Moreover, TRIM46ΔRING-positive MT bundles also show growth recovery in one direction (Figure 3K), demonstrating that the RING finger domain is not involved in parallel MT bundling. Together, these results indicate that TRIM46 forms parallel MT arrays.

TRIM46 Forms Closely Spaced Microtubule Bundles Linked by Thin Cross Bridges

Since TRIM46 specifically localizes to the proximal axon and forms parallel microtubule bundles, we next determined whether TRIM46 can induce the formation of very closed spaced microtubule fascicles, typically observed at the AIS (Leterrier and Dargent, 2014; Rasband, 2010). MT fascicles are only observed by electron microscopy and are comprised of several closely spaced parallel microtubules linked by electron dense cross-bridges (Palay et al., 1968; Peters et al., 1968). While in control cells microtubule bundles are rarely observed, ultrastructural analysis of HeLa cells expressing mCherry-TRIM46 revealed multiple clusters of perpendicular cut MT bundles consisting of ~5–9 individual MT connected by thin cross-bridges (Figures 4A–4D). On average, ~45% of the MTs within a fascicle show clear cross-bridges (Figure 4E). Analyses of the inter-MT distance reveals an even spacing of ~32 nm (Figure 4F), which is very similar for fasciculated MT spacing at the AIS (Palay et al., 1968; Peters et al., 1968). HeLa cells expressing mCherry-PRC1 or other MT-associated proteins, such as MAP2, MAP7, and Tau also showed MT bundles; however, thin cross-bridges were only occasionally observed (Figures 4A–4F). These data demonstrate that TRIM46 is a unique microtubule associated protein in that it can form closely spaced microtubule bundles linked by thin cross bridges.

TRIM46 Is Required for Parallel Microtubule Organization in the Proximal Axon

To determine whether TRIM46 localizes to axonal MTs in polarized hippocampal neurons, we used dSTORM imaging to resolve single MT bundles within the crowded neuronal MT cytoskeleton (Yau et al., 2014). Dual-color dSTORM imaging

Figure 3. TRIM46 Bundles Parallel Microtubules

(A) Schematic diagram of TRIM46 indicating MT association, proximal axon localization, and rescue of the taxol phenotype.

(B) HeLa cells expressing GFP-TRIM46 wild-type or ΔCOS stained for GFP (green) and alpha-tubulin (red). Maximum intensity projection is shown.

(C and D) HeLa cells expressing GFP-TRIM46 stained for GFP (green) and EB1 (red). The P and C indicate the cell periphery and center, respectively.

(E) Quantification of the ratio of EB1 comets at the cell periphery versus the cell center in control HeLa cells (n = 32) and HeLa cells expressing indicated constructs (n = 15–42).

(F and G) Representative stills and a kymograph from a TIRFM time-lapse recording of COS-7 cells expressing mCherry-TRIM46 (red) and GFP-MT+TIP (green). Time is in seconds.

(H) Schematic representation of laser-induced MT severing (LS) experiment.

(I and J) Representative stills and kymographs from a TIRFM time-lapse recording of COS-7 cells expressing GFP-MT+TIP (green) together with mCherry-TRIM46 or mCherry-PRC1 (red). Time is in seconds, where time point 0 is the moment of LS (asterisk).

(K) Quantification of the percentage of outward and inward MT growth after laser-induced MT severing in COS-7 cells expressing indicated constructs (n = 13–20).

Error bars represent SEM. ***$p < 0.001$, comparing Control (E) or mCherry-PRC1 (K) with individual conditions (t test). Scale bar represents 1 μm in (I) and (J), 5 μm in (F), and 10 μm in (B), (C), and (D).

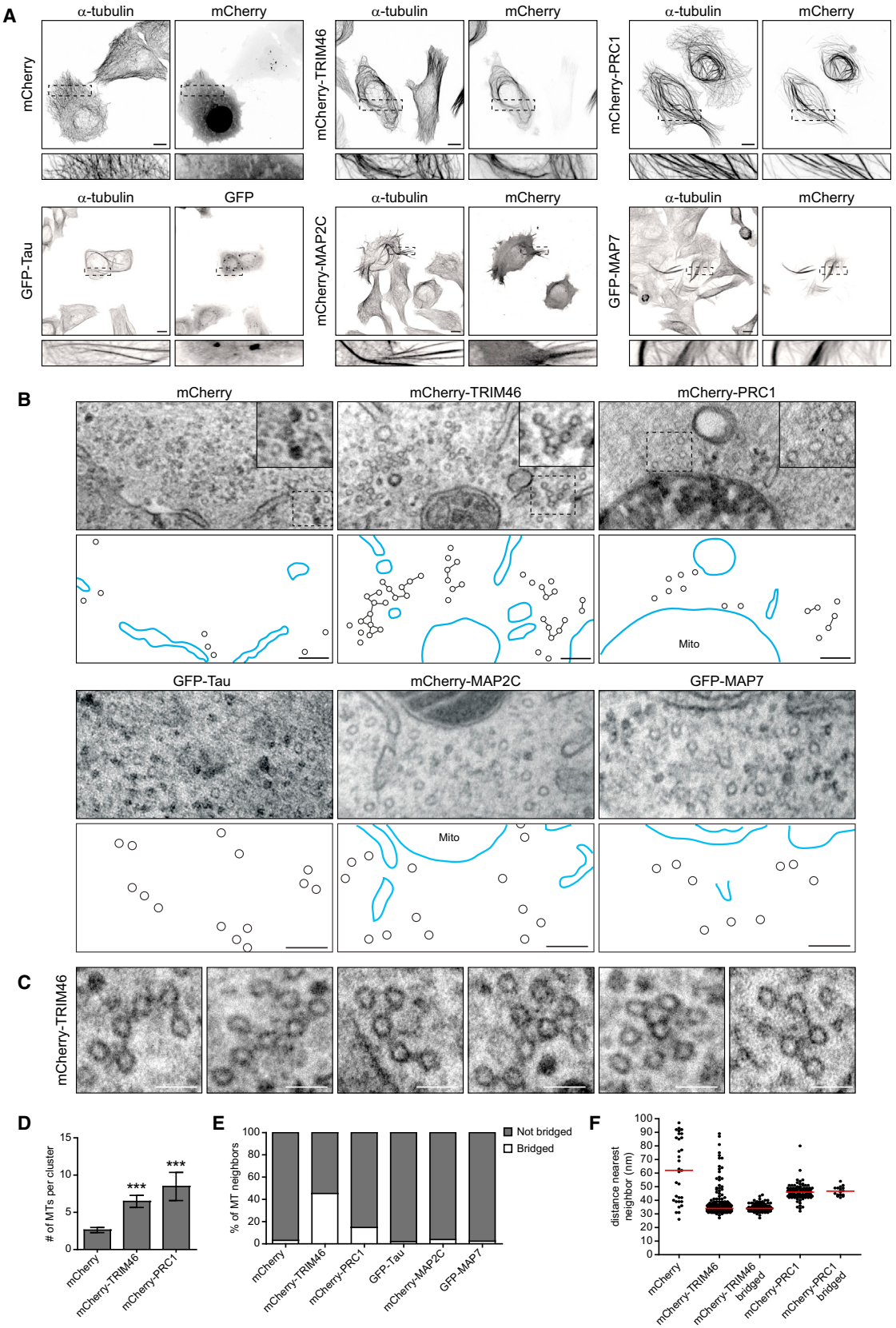

(legend on next page)

revealed that endogenous TRIM46 specifically localizes to MT bundles in the proximal axon (Figures 5A and S4C). To characterize the dynamics of TRIM46 in the proximal axon, we examined the fluorescence recovery after photobleaching (FRAP) of GFP-TRIM46. On average, GFP-TRIM46 fluorescence recovered to 33% of prebleached intensity after ~10 min with an average recovery half-time of 565.6 s (Figures 5B–5D). This recovery of TRIM46 is remarkably slow and incomplete when compared to the MT-associated proteins MAP2 and Tau, which recovered to 85% and 87% of prebleached intensity after ~10 min with an average recovery half-time of 84.8 s and 27.0 s, respectively (Figures 5B–5D). These results indicate that a large fraction of TRIM46 molecules in the proximal axon is highly immobile and that TRIM46 forms a relatively stable compartment in the proximal axon.

We next investigated whether TRIM46 is required for proper axonal MT dynamics and organization. Differentiated neurons transfected with TRIM46 shRNAs stained for EB1 as a marker of dynamic MTs (Jaworski et al., 2009) showed the characteristic comet-like MT plus-end patterns and a normal number of comets in the proximal axon (Figure 5E). Staining of acetylated tubulin as a marker for stable MTs is also unaffected in neurons depleted of TRIM46 (Figure 5F). In addition, FRAP recovery of β-tubulin-GFP in the proximal axon of TRIM46-depleted neurons is similar to control cells (Figure 5G), indicating that TRIM46 is not essential for MT stability in the proximal axon. We next tested whether TRIM46 is required for the unidirectional orientation of axonal MTs. Control neurons show a parallel MT organization with all GFP-MT+TIP comets growing toward the axonal tip (plus-end out) (Figures 5H and 5I; Movie S3). In TRIM46-depleted neurons, the GFP-MT+TIP comets grow in the opposite direction, both toward the axonal tip and the soma (plus-end in) (Figures 5J and 5K; Movie S3). Quantification showed that ~25% of dynamic MTs in TRIM46-depleted neurons are directed with their plus-end toward the cell body, compared to only ~1% plus-end inward orientation in control neurons (Figure 5L). Interestingly, the difference in MT orientations can also be observed in distal axons. No difference in MT growth speed was detected (Figure 5M). Together, these data show that TRIM46 is required for the maintenance of the parallel MT organization in the axon of differentiated neurons.

Polarized Microtubule Arrays Organized by TRIM46 Drive Efficient Axonal Trafficking

Kinesin motor proteins use uniform MT arrays oriented with their plus-end out to drive polarized axonal cargo transport (Kapitein and Hoogenraad, 2011). To directly test whether the uniform axonal MT arrays organized by TRIM46 influence polarized sorting, we made use of an inducible cargo trafficking assay in which we trigger the binding of kinesin motors to peroxisomes during live-cell recordings (Kapitein et al., 2010). Peroxisomes were labeled by expressing PEX-RFP-FKBP, a fusion construct of PEX3 peroxisomal membrane-targeting signal to RFP-FKBP (Figure 6A). FRB is fused to truncated kinesin-1, which contains the motor domain and coiled-coil dimerization region (KIF5-MDC-FRB) (Kapitein et al., 2010). Addition of rapalog to control neurons coexpressing KIF5-MDC-FRB and PEX-RFP-FKBP induced a rapid burst of peroxisomes from the cell body into the axon (Figure 6B), consistent with the selective targeting of kinesin-mediated transport toward MT plus-ends in axons. In the absence of TRIM46, all kinesin-driven peroxisome motilities maintained the selective axonal targeting. Moreover, dynein recruitment retains the selective targeting of peroxisomes to dendrites and no effect was observed in the polarized distribution of the dendritic cargos, such as AMPA receptor subunit GluR2 in neurons depleted for TRIM46 (data not shown). The results indicate that the mixed MT orientations formed in TRIM46 knockdown neurons do not influence polarized cargo trafficking.

We next determined whether uniform axonal MT arrays influence directional axon trafficking and found that the trafficking of kinesin-induced peroxisomes into the axon was markedly reduced in the absence of TRIM46. We analyzed the cargo behavior and found that ~30% of the TRIM46-depleted neurons show axonal peroxisome targeting compared to ~50% of the control neurons (Figures 6C and S7A). We also observed an increased number of stalled vesicles and bidirectional movement in TRIM46 knockdown neurons (Figure 6C). These data are consistent with the analysis of the carrier vesicles containing the axonal protein NgCAM, where ~40% of the NgCAM-GFP vesicles in TRIM46 shRNA-expressing neurons exhibit axonal targeting compared to ~60% of the control cells (Figures 6D and 6E), indicating that antiparallel MT arrays formed in TRIM46-depleted neurons alter axonal cargo transport. We next analyzed in more detail the behavior of axonal vesicle dynamics in TRIM46-depleted neurons. After transfecting cultured hippocampal neurons with GFP-Rab3, as a marker for synaptic vesicle precursors, we followed their movements in axons using high-speed live-cell microscopy (Figures 6F–6I). In control neurons, most GFP-Rab3 vesicles move predominantly in a single direction (Figures 6F and 6G; Movie S4), while in TRIM46 knockdown neurons GFP-Rab3 vesicles switch directions more frequently (Figures 6H and 6I; Movie S4); as a result, the number

Figure 4. TRIM46 Induces Fasciculated Microtubules with Electron-Dense Cross Bridges

(A) HeLa cells expressing indicated constructs and stained for alpha-tubulin.

(B) Representative electron microscopy (EM) acquisitions of HeLa cells expressing the indicated constructs. Microtubules, electron-dense cross-bridges and cellular structures, and mitochondria (Mito) are indicated.

(C) Representative EM acquisitions of HeLa cells expressing mCherry-TRIM46.

(D) Quantification of the microtubule cluster size, defined as being within 100 nm of each other, in HeLa cells expressing indicated constructs (n = 17–41 clusters). Note that the minimum cluster size is 2.

(E) Percentage of nearest neighbors that cross-bridged by electron-dense material in HeLa cells expressing indicated constructs (n = 3–6 cells).

(F) Scatterplot of the nearest neighbor analyses of the clustered microtubules measured from the microtubule center in HeLa cells expressing indicated constructs. The median is in red.

Error bars represent SEM. ***$p < 0.001$, comparing mCherry with individual conditions (Mann-Whitney U test). Scale bar represents 10 μm in (A), 100 nm in (B), and 50 nm in (C).

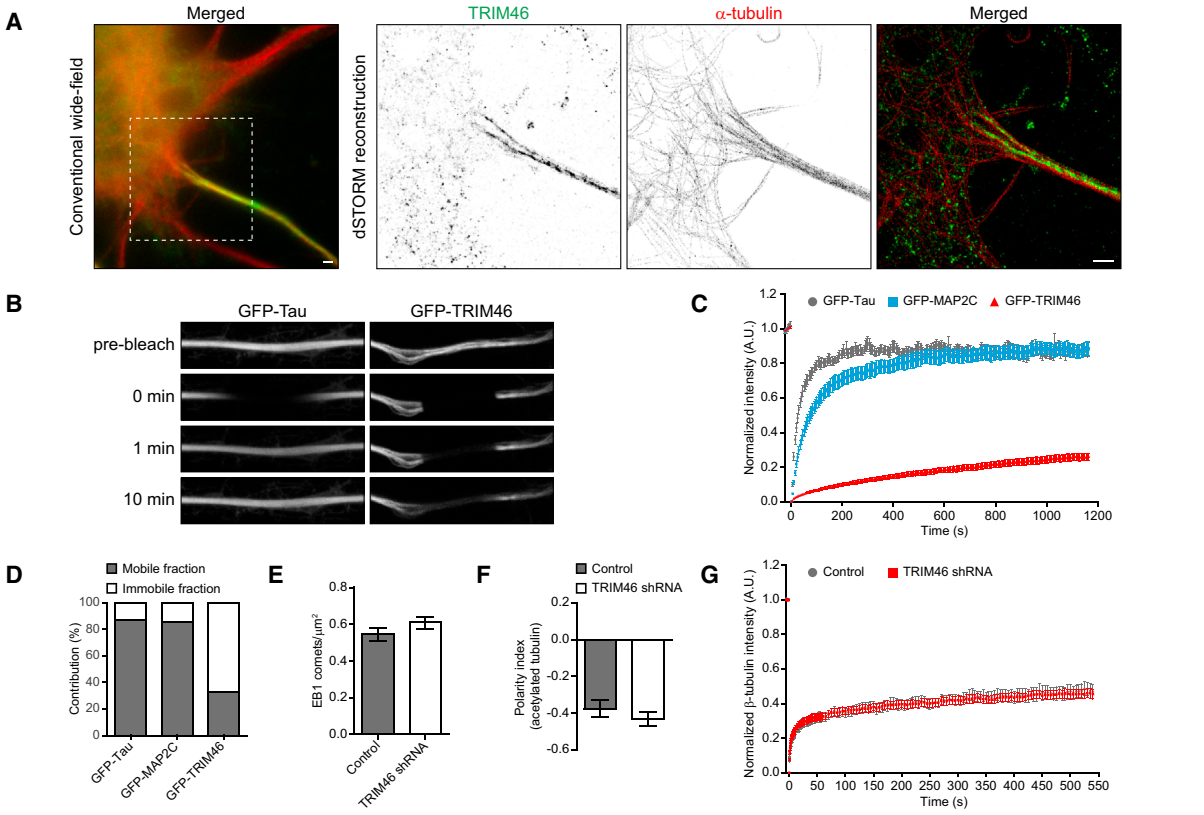

(legend on next page)

of short anterograde and retrograde movements increases (Figure 6J). This can be explained by the mixed orientation of MTs in the axons of TRIM46-depleted neurons. Together, these data suggest that the uniform axon MT arrays organized by TRIM46 drive efficient cargo delivery and trafficking into axons of differentiated neurons.

TRIM46 Is Required for Axon Formation and Neuronal Polarity In Vitro

In contrast to more mature neurons, early neuronal development requires sophisticated architectural changes. It is well known that the polarization of neurons depends on local microtubule reorganization and is characterized by the formation of parallel microtubule arrays (Witte et al., 2008; Yau et al., 2014). To investigate whether TRIM46 is directly involved in this process, we first analyzed the distribution of TRIM46 during the initial polarization of neuronal cells. Following plating, hippocampal neurons pass through a series of morphological stages as they polarize and grow a single axon and several dendrites (Barnes and Polleux, 2009). DIV1 neurons containing a mixed population of stage 2 and stage 3 neurons were fixed and stained for endogenous Tau, AnkG, and TRIM46 (Figure 7A). Stage 2 neurons formed several minor neurites and were found negative for all tested markers, including TRIM46. Significantly, at the stage 2-3 transition, before the future axon grows out and gains its identity, TRIM46 localized to a single neurite. At stage 3, neurons developed a single Tau- and AnkG-positive axon, which all remain positive for TRIM46 as development progresses. Quantification of the mixed stage 2-3 neurons revealed that ~25% of the neurons had a TRIM46-positive, but Tau-negative, neurite and ~70% of the neurons had a TRIM46-positive, but AnkG-negative, neurite (Figure 7B), suggesting that the TRIM46 distribution to the future axon occurred before axon specification and AIS assembly.

To determine whether TRIM46 is involved in neuronal polarization, we knocked down TRIM46 before polarization in stage 1-2 neurons. Directly after dissection, primary cortical neurons were electroporated to deliver TRIM46 shRNA. At DIV4, we determined the number of polarized neurons using the AIS marker AnkG and found a strong reduction in the fraction of polarized cells in TRIM46-depleted cultures compared to controls (Figures 7C and 7D). Depletion of TRIM46 in more mature neurons only partly affected the AIS (Figure S5A), suggesting that TRIM46 is not required for the maintenance of the AIS but necessary for its assembly. To further test whether TRIM46 plays a role in axon initiation and specification, we used the MT-stabilizing drug taxol to induce multiple axons (Witte et al., 2008). In the presence of low concentrations of taxol (20 nM) for 3 days, the number of TRIM46- and AnkG-positive processes per cell was increased more than 5-fold (Figures 7E and 7F). Consistently, TRIM46 localization to the newly formed axon occurs before the assembly of AnkG (Figure 7F). In contrast to taxol treatment, overexpression of GFP-TRIM46 itself does not induce multiple axon formation (Figure 7G). Interestingly, taxol-induced axonal processes positive for Tau and AnkG did not emerge in neurons expressing TRIM46 shRNA (Figures 7E, 7H, and 7I). Axon formation induced by inhibiting the GSK-3β pathway (Yoshimura et al., 2005) was also abolished in TRIM46-depleted neurons (Figure 7J). We next tested which of the TRIM36/46 constructs rescues the taxol phenotype. Overexpression of full-length GFP-TRIM46 restored the taxol-induced knockdown phenotype, while the close homolog GFP-TRIM36 was unable to rescue the TRIM46 shRNA phenotype (Figures 7K and 7L). The N-terminal region of TRIM46 (GFP-TRIM46 ΔC) and the RING finger mutant TRIM46 (GFP-TRIM46-RING mutant) also restored the knockdown phenotype (Figure 7K), indicating that all constructs that target to the proximal axon can also rescue the TRIM46 depletion phenotype (Figure 3A). Together, these in vitro data suggest that specific axonal localization of TRIM46 is required for axon formation; however, the folding and activity of the RING finger is not involved.

TRIM46 Is Required for Axon Formation and Neuronal Polarity In Vivo

Neurons in the developing neocortex migrate from the ventricular zone to the different layers in the cortical plate. During cortical migration, neurons are able to polarize and a trailing process is formed that later becomes the axon (Barnes and Polleux, 2009). To investigate the effect of TRIM46 depletion in cortical neuron migration and axon formation in vivo, we electroporated E14.5 embryos in utero (Figure 8A) and allowed them to develop for 3 more days in the uterus before the embryos were sacrificed and cortical migration was analyzed. Analysis of the cortex from embryos electroporated with control or TRIM46 shRNA, together

Figure 5. TRIM46 Bundles Axonal Parallel Microtubules

(A) Representative image and dSTORM reconstruction of DIV5 hippocampal neurons stained for TRIM46 (green) and alpha-tubulin (red).

(B) FRAP of GFP-Tau or GFP-TRIM46 expressed in hippocampal neurons (DIV11–DIV16) transfected at DIV9–DIV14. Time is in minutes.

(C and D) Average normalized intensity graph of FRAP (C) and the percentage of mobile and immobile fractions after FRAP (D) of indicated constructs (n = 11–12) in neurons (DIV11–DIV16).

(E) Average EB1 density in the proximal axon in fixed hippocampal neurons (DIV5) transfected at DIV1 with pSuper control (n = 21) or TRIM46-shRNA#1/2 (n = 19).

(F) Polarity index of acetylated tubulin in hippocampal neurons (DIV5) transfected at DIV1 with pSuper control (n = 9) or TRIM46-shRNA#1/2 (n = 9).

(G) Average normalized intensity graph of FRAP at the proximal axon of beta-tubulin-GFP co-expressed in hippocampal neurons (DIV5) with pSuper control (n = 7) or TRIM46-shRNA#1/2 (n = 12), transfected at DIV1.

(H–K) Representative still, kymograph, maximal projection zoom, and still zooms from GFP-MT+TIP time-lapse recordings of the axon of hippocampal neurons (DIV4) transfected at DIV1 with GFP-MT+TIP and pSuper control (H and I) or TRIM46-shRNA#1/2 (J and K). Time is in seconds. Anterograde and retrograde growing MT+TIPs are indicated by the green lines/arrows and red lines/arrows, respectively.

(L) Quantification of the percentage anterograde growing MT+TIPs versus retrograde growing MT+TIPs in the axon (total), subdivided in the proximal and distal axon, in hippocampal neurons (DIV4) transfected at DIV1 with GFP-MT+TIP and pSuper control (n = 25 cells) or TRIM46-shRNA#1/2 (n = 26 cells).

(M) Quantification of the growth speed of anterograde and retrograde growing MT +TIPs in hippocampal neurons (DIV4) transfected at DIV1 with GFP-MT+TIP and pSuper control (anterograde only) (n = 25 cells) or TRIM46-shRNA#1/2 (n = 26 cells).

Error bars represent SEM. ***$p < 0.001$ comparing control versus shRNA#1/2 (t test). a.u., arbitrary units. Scale bar represents 1 μm in (A) and 10 μm in (H) and (J).

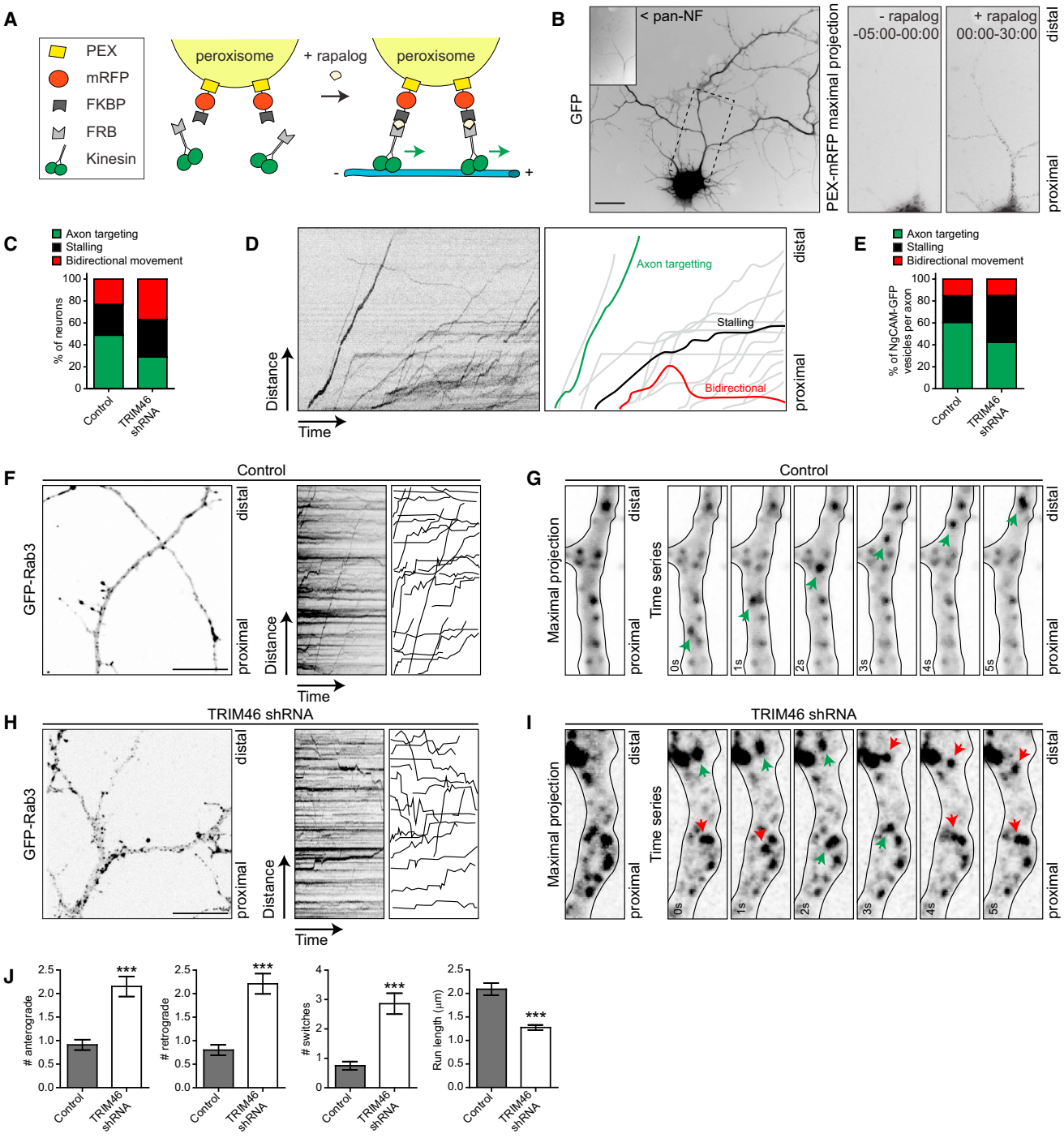

Figure 6. Parallel Microtubule Bundling in the Axon by TRIM46 Is Essential for Normal Axonal Transport

(A) Schematic representation of specific kinesin targeting to peroxisomes using the FKBP-FRB rapalog-induced dimerization system.

(B and C) Representative images (B) and quantification (C) of hippocampal neurons (DIV5) transfected at DIV1 with HA-KIF5-MDC-FRB, PEX-mRFP-FKBP, GFP, and pSuper control (n = 45) or TRIM46-shRNA#1/2 (n = 51). Extracellular pan-NF is used to identify the axon. Time mm:ss. Quantification shows the percentage of neurons classified by different behavior of Kif5b-targeted peroxisomes.

(D and E) Representative kymograph (D) and quantification (E) of single GFP-NgCAM vesicle behavior in the proximal axon of hippocampal neurons (DIV10) transfected at DIV7 with GFP-NgCAM and pSuper control (n = 21) or TRIM46-shRNA#1/2 (n = 18). The highlighted projections of the kymograph represent the different categories.

(legend continued on next page)

with a GFP plasmid, revealed that GFP-positive control neurons efficiently migrated to the upper layers of the cortical plate (Figures 8B and 8D). In contrast, many GFP-positive neurons expressing TRIM46 shRNA failed to migrate properly and accumulated in the intermediate zone (Figures 8C and 8D). Detailed analysis shows that the migrating GFP-positive control neurons have a stereotypical bipolar morphology with a leading process and a trailing edge (Figure 8E). However, TRIM46-depleted GFP-positive neurons do not show this stereotypical morphology. They did not typically form a leading process and a long trailing process that will form the future axon (Figure 8F). Quantification showed that ~81% of the control neurons possess a typical axonal process in contrast to only ~38% of the TRIM46 knockdown neurons (Figures 8G and 8H). Expression of full-length GFP-TRIM46 partly rescued the TRIM46 shRNA phenotypes, while the GFP-TRIM46ΔRing construct was unable to restore migration and axon formation (Figures 8D–8H and S8). Consistent with the in vitro data, the RING finger mutant TRIM46 (GFP-TRIM46-RING mutant) also restored the knockdown phenotype (Figures 8D–8H and S8). In addition, at postnatal stages of development (P5), TRIM46-depleted neurons in the neocortex did not form an axon and lack AnkG staining (Figures 8I and 8J). Together, these data demonstrate that TRIM46 is required for axon formation and establishment of neuronal polarity and proper neuronal migration in vivo.

DISCUSSION

Here we describe a molecular mechanism that controls uniform MT orientation in axons. We demonstrate that TRIM46 specifically localizes to the proximal axon and forms closely spaced parallel MT bundles. TRIM46 is required for uniform MT orientation in axons and neuronal polarity in vitro and in vivo. Moreover, we show that the parallel MT arrays drive efficient cargo delivery and trafficking. Our data suggest that TRIM46 defines a specific axonal compartment for regulating MT organization and cargo transport.

TRIM46 Is Required for Neuronal Polarization and Axon Formation

The MT cytoskeleton is required for the initial polarization of neuronal cells (Conde and Cáceres, 2009; Hoogenraad and Bradke, 2009). Here we show that neurons lacking the MT-associated protein TRIM46 fail to initiate axon formation and show impaired neuronal polarization during in vitro and in vivo development. Since TRIM46 is needed for uniform MT orientation in axons, these data suggest that forming parallel MT arrays in the axon plays a critical role during the specification of axonal fate in early neuronal development. We found that TRIM46 is an early marker for neuronal polarization because it localizes to the future axon before axon specification and AIS assembly. In addition, MT stabilization has been shown to be important for initial neuronal polarization (Witte et al., 2008). The MT minus-end binding protein CAMSAP2, which stabilizes MT minus-ends, is enriched in the very first part of the axon but is absent from the TRIM46-positive region (Yau et al., 2014). High levels of CAMSAP2 at the base of the axon may create a local pool of stabilized MT minus-ends and promote plus-end out-oriented MT growth in axons. TRIM46 may subsequently organize the newly formed MT into uniform plus-end out MT bundles. We propose a model in which both local MT stabilization and formation of uniform MTs in the axonal shaft can directly affect the polarity of neurons. Since axonal MTs need to point with the plus-ends toward the growth cone in order to induce axonal growth (Witte et al., 2008), it is tempting to speculate that organizing axonal MTs in parallel bundles leads to an accumulation of dynamic MT plus-ends at the neurite tips, resulting in net elongation of the axon. Indeed, TRIM46 depleted in neurons at later stages of differentiation still showed reduced axonal outgrowth. Interestingly in this respect is that the mixed MT orientations in TRIM46-depleted neurons can also be observed in distal axons. MT transport and sliding mechanisms have been suggested for organizing axonal microtubules (Baas and Lin, 2011; Lu et al., 2013) and TRIM46 could potentially be involved in MT organization at the beginning of the axon. Alternatively, neuronal polarity could be stimulated by directional transport mechanisms along uniform MT arrays in the axon. The parallel organization of the MTs may promote delivery of cargo vesicles to the axon or even certain polarity factors that directly contribute to axonal fate. Indeed, we found uniform axon MT arrays organized by TRIM46 to drive efficient cargo delivery and trafficking. Future work will be needed to resolve the molecular interplay between MT stabilization and the bundling of parallel MTs in the axon during early neuronal polarization.

TRIM46 Defines a Specific Region at the Proximal Axon

After the initial polarization, the proximal axon builds up the AIS required for neuronal physiology and to maintain neuronal polarity (Leterrier and Dargent, 2014; Rasband, 2010). The AIS has been shown to function as a diffusion barrier for both cytoplasmic and membrane proteins and as a gate keeper for axon-specific cargo transport (Kapitein et al., 2010; Nakada et al., 2003; Petersen et al., 2014; Song et al., 2009; Watanabe et al., 2012). Here we show that MT-associated protein TRIM46 specifically localizes to the proximal axon, which partly overlaps with the AIS. Interestingly, TRIM46 is the first AIS

(F–I) Representative still, kymograph, maximal projection zoom, and still zooms from GFP-Rab3 time-lapse recordings of the axon of hippocampal neurons (DIV4) transfected at DIV1 with GFP-Rab3 and pSuper control (F and G) or TRIM46-shRNA#1/2 (H and I). Time is in seconds. Anterograde and retrograde moving vesicles are indicated by the green arrows and red arrows, respectively.

(J) Quantification of the behavior of processive GFP-Rab3 vesicles within 60 s in the axon of hippocampal neurons (DIV4) transfected at DIV1 with GFP-Rab3 and pSuper control (n = 11 cells) or TRIM46-shRNA#1/2 (n = 14 cells). # anterograde, mean number of periods that vesicles move anterograde. # retrograde, mean number of periods that vesicles move retrograde. # switches, mean number of times that vesicles switch between anterograde and retrograde movements. Run lengths, mean run length of a vesicle in a single direction.

Error bars represent SEM. Comparing control versus shRNA#1/2 (Mann-Whitney U test): axon targeting $p < 0.01$, stalling $p < 0.01$, bidirectional not significant in (E); ***$p < 0.001$ in (J). Scale bar represents 10 μm in (B), (F), and (H).

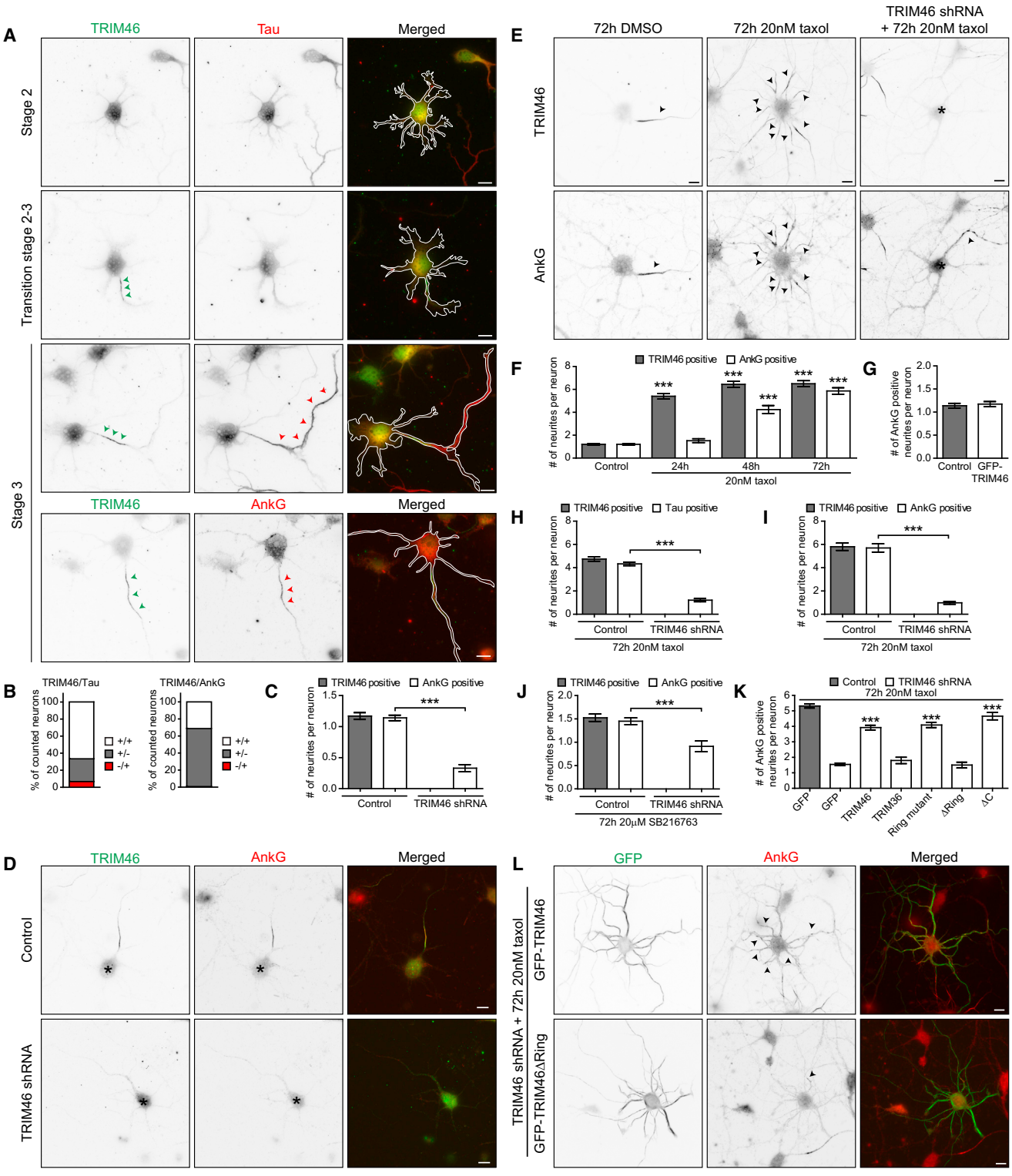

Figure 7. TRIM46 Is Required for Neuronal Polarity and Axon Formation

(A) Different stages of cultured hippocampal neurons (DIV1) stained for TRIM46 (green) and Tau or AnkG (red).

(B) Quantification of the percentage of neurons at DIV1 with neurites positive/negative for TRIM46/Tau (n = 165) and TRIM46/AnkG (n = 150).

(C and D) Quantification (C) and representative images (D) of DIV4 cortical neurons electroporated before plating with pSuper control (n = 100) or TRIM46-shRNA#1/2 (n = 100), and co-stained with TRIM46 (green) and AnkG (red).

(legend continued on next page)

protein that is not also found at nodes of Ranvier in the sciatic nerves. Consistently, MT fasciculation is also absent in the nodes of Ranvier in these motor axons (Nakazawa and Ishikawa, 1995). It will be interesting to stain for TRIM46 at nodes of Ranvier that have been reported to contain MT fasciculation, such as in sensory axons. Although AnkG and TRIM46 mark distinct axonal domains and control different molecular mechanisms, they function in interdependent pathways. During neuronal polarization, TRIM46 localizes to the newly formed axon before AnkG clustering and is required for the assembly of the AIS in developing neurons. Knockdown of AnkG in more mature neurons causes a marked TRIM46 redistribution, which is consistent with the general role of AnkG in the maintenance of axo-dendritic polarity (Hedstrom et al., 2008; Sobotzik et al., 2009). TRIM46 and AnkG are both required for the polarized distribution of somatodendritic MAP2 and axonal Tau (Hedstrom et al., 2008; Sobotzik et al., 2009). It is possible that TRIM46 forms a MT-based boundary between MAP2 and Tau, which is stably maintained by the AIS. Recent data showed that the barrier required for axonal retention of Tau does not directly involves the AIS function (Li et al., 2011). Since filtering of cytoplasmic traffic at the AIS largely depends on the underlying actin cytoskeleton (Song et al., 2009; Watanabe et al., 2012), it is possible that the role of TRIM46 is distinct from the AIS as gatekeeper for controlling polarized cargo transport. Indeed, cargos keep their polarized distribution in neurons depleted for TRIM46. It is tempting to speculate that TRIM46 may be involved the pathological mislocalization of Tau in neurodegenerative diseases (Zempel and Mandelkow, 2014).

TRIM46 Forms the Parallel Microtubule Arrays of Axons

The other C-I TRIM family members, including TRIM-9, TRIM-36, MID1, and MID2, all associate with MTs and have E3 ubiquitin ligase activity (Short and Cox, 2006). Although TRIM36 forms parallel MTs, it does not target the proximal axon and is unable to rescue the TRIM46 depletion phenotype. We found that the sequences within the TRIM46 RING finger domain and MT binding properties of the COS box are collectively involved in the axon localization. In addition, the folding and activity of the RING finger domain is dispensable for TRIM46 function, suggesting that TRIM46 is an unusual C-I TRIM subfamily member that not necessarily exhibits E3 ubiquitin ligase activity. Interestingly, the MT-associated protein MID related protein 1 (MIR1/FSD1), which contains the COS box and other C-terminal TRIM46 domains, has completely lost the RING and B-box motifs (Stein et al., 2002). Functional characterization of TRIM46 in neurons highlights the evolutionary dynamics of the TRIM family and reveals new aspects of the RING domain in the axon specific targeting.

It remains, however, unclear how TRIM46 is specifically targeted to the proximal axon. It is possible that TRIM46 favors specific MT post-translational modifications or tubulin isotypes that are only present at the proximal axon, even though none of the known modifications mark this specific axonal compartment (Janke and Kneussel, 2010). Alternatively, TRIM46 may prefer to bind to the stable MT population in the axon (Nakata et al., 2011; Witte et al., 2008), which is supported by the observation that TRIM46 promptly localized to multiple neurites after stabilizing MTs by low concentrations of taxol. It is also possible that TRIM46's axonal accumulation is achieved by a self-organized assembly on a subset of axonal MTs, as proposed for many other MT-associated proteins (Subramanian and Kapoor, 2012). TRIM family proteins are known to self-associate by forming anti-parallel dimers and other higher-order complexes, and the RING domain is important in this process (Li et al., 2014; Sanchez et al., 2014). It is tempting to speculate that parallel MT crosslinking may be achieved by cooperative interactions between TRIM46 molecules along axonal MTs. Consistently, TRIM46 forms stable structures in the proximal axon and induces microtubule fascicles with electron-dense cross-bridges in HeLa cells. It is possible that TRIM46 resembles the characteristic cross-bridges observed between the closely spaced parallel microtubules at the AIS (Palay et al., 1968; Peters et al., 1968). Further insights into parallel MT crosslinking mechanisms are likely to come from the analysis of TRIM46 knockout mice and in vitro reconstitution studies with purified proteins and structural analyses.

In summary, we demonstrate that TRIM46 defines a unique axonal cytoskeletal compartment for regulating MT organization and directional cargo transport during neuronal development. By forming uniform MT bundles in the axon, TRIM46 is required for neuronal polarity and axon specification in vitro and in vivo. As parallel MT arrays are critically important for many other axonal functions in mature neurons, including presynaptic plasticity and axon regeneration, we anticipate that more processes that involve TRIM46 will be revealed in the future. Moreover, the role of TRIM46 in localizing voltage-gated sodium (Nav) channels and generating action potentials at the AIS needs to be determined. Alterations in axonal MT organization and cargo trafficking have been described in several neurodegenerative diseases (Millecamps and Julien, 2013; Zempel and Mandelkow, 2014). Our current findings also provide new molecular targets to investigate defects in the sorting machinery in neurodegenerative disease models.

(E and F) Representative images (E) and quantification (F) of DIV7 hippocampal neurons treated at DIV4 with control vehicle (DMSO, 72 hr) or 20 nM taxol for different time points (n = 50 per condition). Neurons were co-stained with TRIM46 and AnkG.

(G) Quantification of DIV4 hippocampal neurons transfected at DIV1 with GFP-TRIM46 and stained with AnkG.

(H–J) Quantification of TRIM46 and Tau (H) or AnkG (I and J) staining in hippocampal neurons (DIV7) transfected at DIV1 with pSuper control (H, n = 70; I, n = 50; J, n = 80) or TRIM46-shRNA#1/2 (H, n = 43; I, n = 50; J, n = 46), treated at DIV4 for 72 hr with 20 nM taxol (H and I) or 20 μM SB216763 (J).

(K and L) Quantification of representative images of hippocampal neurons (DIV7) transfected at DIV1 with pSuper control or TRIM46-shRNA#1/2, together with indicated constructs (n = 60–305) and treated at DIV4 with 20 nM taxol for 72 hr and stained for AnkG (red).

Error bars represent SEM. ***$p < 0.001$ comparing (unless differently indicated) control versus individual conditions (Mann-Whitney U test) for (C), (F), (H), (I), and (J). ***$p < 0.001$ comparing GFP + shRNA#1/2 versus the different rescues in shRNA#1/2 (t test) for (K). Asterisks in images mark positively transfected cell in (D) and (E). Arrowheads indicate the axon formation (AnkG based) in (E) and (L). Scale bar represents 10 μm in (A), (D), (E) and (L).

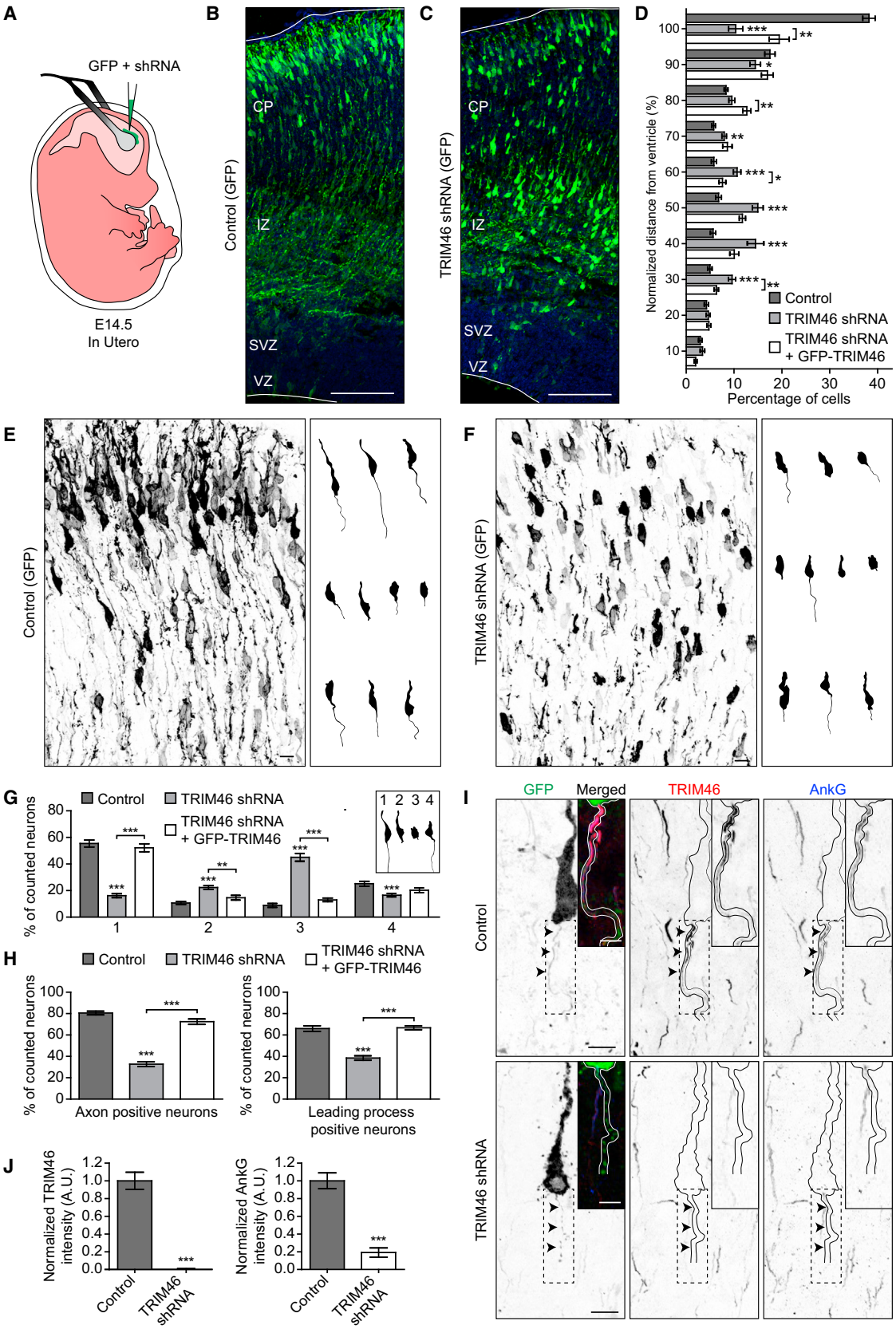

(legend on next page)

EXPERIMENTAL PROCEDURES

DNA and shRNA Constructs

TRIM46 and TRIM36 clones were both kindly provided by Dr. T.Cox (Short and Cox, 2006). All TRIM expression constructs were generated by a PCR-based strategy and placed in different expression vectors. The following TRIM46 shRNAs were designed and used in this study: rat TRIM46-shRNA 1 (5′-gtt gctgacagagcttaac-3′), mouse TRIM46-shRNA 1 (5′-gctgttgaccgagcttagc-3′), and rat/mouse TRIM46-shRNA 2 (5′-gaacatggagaaggaactg-3′). For further details, see Supplemental Experimental Procedures.

Antibodies and Reagents

Autoimmune serum used in this study are described by Shams'ili et al. (2009) and Sabater et al. (2013). Rabbit anti-TRIM46 was made by injecting full-length GST-TRIM46 (precipitated in PBS) together with adjuvant into New Zealand White rabbits (by BioGenes GmbH). TRIM46 antibodies were used for western blot, immunohisto- and immunocytochemistry experiments. For further details see Supplemental Experimental Procedures.

Primary Hippocampal and Cortical Neuron Cultures, Transfection, and Immunocytochemistry

Primary hippocampal and cortical cultures were isolated from embryonic day 18 (E18) rat brains. Hippocampal cultures were transfected using Lipofectamine 2000 (Life Technologies) and cortical cultures using the Amaxa Rat Neuron Nucleofector kit (Lonza). For further details see Supplemental Experimental Procedures.

Imaging

The following microscopy techniques were used for live cell imaging and immunohisto- and immunocytochemistry: total internal reflection fluorescence microscopy (TIRFM), spinning-disc confocal microscopy, laser-induced cutting using TIRFM, wide-field fluorescence microscopy, and confocal laser-scanning microscopy. For details, see Supplemental Experimental Procedures.

SUPPLEMENTAL INFORMATION

Supplemental Information includes Supplemental Experimental Procedures, eight figures, and four movies and can be found with this article online at http://dx.doi.org/10.1016/j.neuron.2015.11.012.

AUTHOR CONTRIBUTIONS

S.F.B.v.B cloned DNA constructs, designed and performed biochemical and imaging experiments, analyzed results, and wrote the manuscript; L.W. performed immunohistochemistry experiments; A.C. performed dSTORM and tubulin FRAP experiments and analyzed the results; E.Y.v.B. performed the in utero surgery procedure; M.A.M.F. performed the rapalog-inducible cargo trafficking assay in neurons and analyzed the results; C.P.F. performed the axon morphology analysis; E.A.K. made the MATLAB analysis scripts used for analysis; M.H., K.V., L.S., J.A.P., performed EM and analyzed data; A.T.A. cloned DNA constructs and performed localization experiments; S.D. cloned DNA and shRNA constructs; P.S.S. provided autoimmune serum #1, R.J.P. supervised in utero experiments; R.S, A.F.M.A. performed and analyzed mass spectrometry data, A.A. gave advice throughout the project and edited the manuscript; L.C.K. supervised dSTORM experiments; E.d.G. cloned DNA and shRNA constructs, performed knockdown staining experiments, supervised the research, and wrote the manuscript; C.C.H. supervised the research, coordinated the study, and wrote the manuscript.

ACKNOWLEDGMENTS

We thank Dr. F. Graus for sharing the autoimmune sera, Dr. M. Rasband for the βIV-Spectrin antibodies, Dr. T. Cox for the TRIM-constructs, and Dr. M. Boxem for the PRC1 clones. We thank Dr. D. Jaarsma and R. van den Berg for their help with immunohistochemistry experiments, Willine van de Wetering and Elly van Donselaar for their help and advice with electron microscopy, and Dr. B. Snel for the help with phylogenetic analysis. This work was supported by the Netherlands Organization for Scientific Research (NWO-ALW-VICI, C.C.H.), the Foundation for Fundamental Research on Matter ((FOM) C.C.H.), which is part of the NWO, the Netherlands Organization for Health Research and Development (ZonMW-TOP, CCH), the European Research Council (ERC) (ERC-consolidator, C.C.H.), Cyttron II (FES0908, K.V., J.A.P.). This research was partly performed within the framework of CTMM, the Center for Translational Molecular Medicine, project EMINENCE (01C-204) (R.J.P.), and supported by the Marie Curie Initial Training Network (MC-ITN).

Received: February 18, 2015
Revised: September 13, 2015
Accepted: November 3, 2015
Published: December 3, 2015

REFERENCES

Baas, P.W., and Ahmad, F.J. (2013). Beyond taxol: microtubule-based treatment of disease and injury of the nervous system. Brain *136*, 2937–2951.

Baas, P.W., and Lin, S. (2011). Hooks and comets: The story of microtubule polarity orientation in the neuron. Dev. Neurobiol. *71*, 403–418.

Baas, P.W., Deitch, J.S., Black, M.M., and Banker, G.A. (1988). Polarity orientation of microtubules in hippocampal neurons: uniformity in the axon and nonuniformity in the dendrite. Proc. Natl. Acad. Sci. USA *85*, 8335–8339.

Barnes, A.P., and Polleux, F. (2009). Establishment of axon-dendrite polarity in developing neurons. Annu. Rev. Neurosci. *32*, 347–381.

Berghs, S., Ferracci, F., Maksimova, E., Gleason, S., Leszczynski, N., Butler, M., De Camilli, P., and Solimena, M. (2001). Autoimmunity to beta IV spectrin in paraneoplastic lower motor neuron syndrome. Proc. Natl. Acad. Sci. USA *98*, 6945–6950.

Figure 8. TRIM46 Is Required for Axon Formation In Vivo

(A) Schematic representation of the in utero electroporation procedure.

(B–D) Low-magnification stitched maximum intensity projection (GFP) and quantification of migrating neurons in E17.5 mouse cortex which were positively in utero electroporated (E14.5) with GFP and pSuper control (n = 31) (B), TRIM46-shRNA#1/2 (n = 33), or TRIM46-shRNA#1/2 and GFP-TRIM46 (shRNA non-targetable) (n = 19) (C). Quantification (D) shows the normalized migration distribution along the radial axis from the ventricle to the pial surface of GFP-positive neurons. CP, cortical plate; IZ, intermediate zone; SVZ, subventricular zone; VZ, ventricular zone.

(E–H) Higher-magnification maximum intensity projection (GFP) and quantification of E17.5 mouse cortex which were in utero electroporated (E14.5) with GFP and pSuper control (n = 34) (E), TRIM46-shRNA#1/2 (n = 35), or TRIM46-shRNA#1/2 and GFP-TRIM46 (shRNA non-targetable) (n = 21) (F). Right panels in (E) and (F) show individual traces of representative GFP-positive neurons. Quantifications show the distribution of four different GFP-positive neuronal cell morphologies (G), and the percentage of axon-positive (H, left) and/or leading process-positive (H, right) neurons (GFP positive).

(I and J) Representative maximum intensity projection (I) and quantification (J) of P5 mouse cortex that were in utero electroporated (E14.5) with GFP and pSuper control (n = 15), or TRIM46-shRNA#1/2 (n = 14).

Error bars represent SEM. *$p < 0.05$, **$p < 0.01$, ***$p < 0.001$, comparing corresponding bins in (D), neuron type in (G) and (H), or normalized intensity in (J) of (unless differently indicated) control versus shRNA#1/2 (Mann-Whitney U test). a.u., arbitrary units. Scale bar represents 100 μm in (B), (C), (E), and (F), 10 μm in (I), and 5 μm in (I) zoom.

Bradke, F., Fawcett, J.W., and Spira, M.E. (2012). Assembly of a new growth cone after axotomy: the precursor to axon regeneration. Nat. Rev. Neurosci. *13*, 183–193.

Chisholm, A.D. (2013). Cytoskeletal dynamics in Caenorhabditis elegans axon regeneration. Annu. Rev. Cell Dev. Biol. *29*, 271–297.

Conde, C., and Cáceres, A. (2009). Microtubule assembly, organization and dynamics in axons and dendrites. Nat. Rev. Neurosci. *10*, 319–332.

de Graaff, E., Maat, P., Hulsenboom, E., van den Berg, R., van den Bent, M., Demmers, J., Lugtenburg, P.J., Hoogenraad, C.C., and Sillevis Smitt, P. (2012). Identification of delta/notch-like epidermal growth factor-related receptor as the Tr antigen in paraneoplastic cerebellar degeneration. Ann. Neurol. *71*, 815–824.

Deshaies, R.J., and Joazeiro, C.A. (2009). RING domain E3 ubiquitin ligases. Annu. Rev. Biochem. *78*, 399–434.

Hammond, J.W., Huang, C.F., Kaech, S., Jacobson, C., Banker, G., and Verhey, K.J. (2010). Posttranslational modifications of tubulin and the polarized transport of kinesin-1 in neurons. Mol. Biol. Cell *21*, 572–583.

Hedstrom, K.L., Ogawa, Y., and Rasband, M.N. (2008). AnkyrinG is required for maintenance of the axon initial segment and neuronal polarity. J. Cell Biol. *183*, 635–640.

Hoogenraad, C.C., and Bradke, F. (2009). Control of neuronal polarity and plasticity–a renaissance for microtubules? Trends Cell Biol. *19*, 669–676.

Huang, N.J., Zhang, L., Tang, W., Chen, C., Yang, C.S., and Kornbluth, S. (2012). The Trim39 ubiquitin ligase inhibits APC/CCdh1-mediated degradation of the Bax activator MOAP-1. J. Cell Biol. *197*, 361–367.

Ikeda, K., and Inoue, S. (2012). TRIM proteins as RING finger E3 ubiquitin ligases. Adv. Exp. Med. Biol. *770*, 27–37.

Janke, C., and Kneussel, M. (2010). Tubulin post-translational modifications: encoding functions on the neuronal microtubule cytoskeleton. Trends Neurosci. *33*, 362–372.

Jaworski, J., Kapitein, L.C., Gouveia, S.M., Dortland, B.R., Wulf, P.S., Grigoriev, I., Camera, P., Spangler, S.A., Di Stefano, P., Demmers, J., et al. (2009). Dynamic microtubules regulate dendritic spine morphology and synaptic plasticity. Neuron *61*, 85–100.

Kapitein, L.C., and Hoogenraad, C.C. (2011). Which way to go? Cytoskeletal organization and polarized transport in neurons. Mol. Cell. Neurosci. *46*, 9–20.

Kapitein, L.C., Schlager, M.A., Kuijpers, M., Wulf, P.S., van Spronsen, M., MacKintosh, F.C., and Hoogenraad, C.C. (2010). Mixed microtubules steer dynein-driven cargo transport into dendrites. Curr. Biol. *20*, 290–299.

Kleele, T., Marinković, P., Williams, P.R., Stern, S., Weigand, E.E., Engerer, P., Naumann, R., Hartmann, J., Karl, R.M., Bradke, F., et al. (2014). An assay to image neuronal microtubule dynamics in mice. Nat. Commun. *5*, 4827.

Leterrier, C., and Dargent, B. (2014). No Pasaran! Role of the axon initial segment in the regulation of protein transport and the maintenance of axonal identity. Semin. Cell Dev. Biol. *27*, 44–51.

Li, X., Kumar, Y., Zempel, H., Mandelkow, E.M., Biernat, J., and Mandelkow, E. (2011). Novel diffusion barrier for axonal retention of Tau in neurons and its failure in neurodegeneration. EMBO J. *30*, 4825–4837.

Li, Y., Wu, H., Wu, W., Zhuo, W., Liu, W., Zhang, Y., Cheng, M., Chen, Y.G., Gao, N., Yu, H., et al. (2014). Structural insights into the TRIM family of ubiquitin E3 ligases. Cell Res. *24*, 762–765.

Loïodice, I., Staub, J., Setty, T.G., Nguyen, N.P., Paoletti, A., and Tran, P.T. (2005). Ase1p organizes antiparallel microtubule arrays during interphase and mitosis in fission yeast. Mol. Biol. Cell *16*, 1756–1768.

Lu, W., Fox, P., Lakonishok, M., Davidson, M.W., and Gelfand, V.I. (2013). Initial neurite outgrowth in Drosophila neurons is driven by kinesin-powered microtubule sliding. Curr. Biol. *23*, 1018–1023.

Maday, S., Twelvetrees, A.E., Moughamian, A.J., and Holzbaur, E.L. (2014). Axonal transport: cargo-specific mechanisms of motility and regulation. Neuron *84*, 292–309.

Millecamps, S., and Julien, J.P. (2013). Axonal transport deficits and neurodegenerative diseases. Nat. Rev. Neurosci. *14*, 161–176.

Nakada, C., Ritchie, K., Oba, Y., Nakamura, M., Hotta, Y., Iino, R., Kasai, R.S., Yamaguchi, K., Fujiwara, T., and Kusumi, A. (2003). Accumulation of anchored proteins forms membrane diffusion barriers during neuronal polarization. Nat. Cell Biol. *5*, 626–632.

Nakata, T., and Hirokawa, N. (2003). Microtubules provide directional cues for polarized axonal transport through interaction with kinesin motor head. J. Cell Biol. *162*, 1045–1055.

Nakata, T., Niwa, S., Okada, Y., Perez, F., and Hirokawa, N. (2011). Preferential binding of a kinesin-1 motor to GTP-tubulin-rich microtubules underlies polarized vesicle transport. J. Cell Biol. *194*, 245–255.

Nakazawa, E., and Ishikawa, H. (1995). Occurrence of fasciculated microtubules at nodes of Ranvier in rat spinal roots. J. Neurocytol. *24*, 399–407.

Napolitano, L.M., Jaffray, E.G., Hay, R.T., and Meroni, G. (2011). Functional interactions between ubiquitin E2 enzymes and TRIM proteins. Biochem. J. *434*, 309–319.

Notturno, F., Di Febo, T., Yuki, N., Fernandez Rodriguez, B.M., Corti, D., Nobile-Orazio, E., Carpo, M., De Lauretis, A., and Uncini, A. (2014). Autoantibodies to neurofascin-186 and gliomedin in multifocal motor neuropathy. J. Neuroimmunol. *276*, 207–212.

Palay, S.L., Sotelo, C., Peters, A., and Orkand, P.M. (1968). The axon hillock and the initial segment. J. Cell Biol. *38*, 193–201.

Peters, A., Proskauer, C.C., and Kaiserman-Abramof, I.R. (1968). The small pyramidal neuron of the rat cerebral cortex. The axon hillock and initial segment. J. Cell Biol. *39*, 604–619.

Petersen, J.D., Kaech, S., and Banker, G. (2014). Selective microtubule-based transport of dendritic membrane proteins arises in concert with axon specification. J. Neurosci. *34*, 4135–4147.

Rasband, M.N. (2010). The axon initial segment and the maintenance of neuronal polarity. Nat. Rev. Neurosci. *11*, 552–562.

Sabater, L., Höftberger, R., Boronat, A., Saiz, A., Dalmau, J., and Graus, F. (2013). Antibody repertoire in paraneoplastic cerebellar degeneration and small cell lung cancer. PLoS ONE *8*, e60438.

Sanchez, J.G., Okreglicka, K., Chandrasekaran, V., Welker, J.M., Sundquist, W.I., and Pornillos, O. (2014). The tripartite motif coiled-coil is an elongated antiparallel hairpin dimer. Proc. Natl. Acad. Sci. USA *111*, 2494–2499.

Schwamborn, J.C., Berezikov, E., and Knoblich, J.A. (2009). The TRIM-NHL protein TRIM32 activates microRNAs and prevents self-renewal in mouse neural progenitors. Cell *136*, 913–925.

Shams'ili, S., de Leeuw, B., Hulsenboom, E., Jaarsma, D., and Smitt, P.S. (2009). A new paraneoplastic encephalomyelitis autoantibody reactive with the axon initial segment. Neurosci. Lett. *467*, 169–172.

Short, K.M., and Cox, T.C. (2006). Subclassification of the RBCC/TRIM superfamily reveals a novel motif necessary for microtubule binding. J. Biol. Chem. *281*, 8970–8980.

Sobotzik, J.M., Sie, J.M., Politi, C., Del Turco, D., Bennett, V., Deller, T., and Schultz, C. (2009). AnkyrinG is required to maintain axo-dendritic polarity in vivo. Proc. Natl. Acad. Sci. USA *106*, 17564–17569.

Song, A.H., Wang, D., Chen, G., Li, Y., Luo, J., Duan, S., and Poo, M.M. (2009). A selective filter for cytoplasmic transport at the axon initial segment. Cell *136*, 1148–1160.

Stein, P.A., Toret, C.P., Salic, A.N., Rolls, M.M., and Rapoport, T.A. (2002). A novel centrosome-associated protein with affinity for microtubules. J. Cell Sci. *115*, 3389–3402.

Stepanova, T., Slemmer, J., Hoogenraad, C.C., Lansbergen, G., Dortland, B., De Zeeuw, C.I., Grosveld, F., van Cappellen, G., Akhmanova, A., and Galjart, N. (2003). Visualization of microtubule growth in cultured neurons via the use of EB3-GFP (end-binding protein 3-green fluorescent protein). J. Neurosci. *23*, 2655–2664.

Stone, M.C., Roegiers, F., and Rolls, M.M. (2008). Microtubules have opposite orientation in axons and dendrites of Drosophila neurons. Mol. Biol. Cell *19*, 4122–4129.

Subramanian, R., and Kapoor, T.M. (2012). Building complexity: insights into self-organized assembly of microtubule-based architectures. Dev. Cell *23*, 874–885.

Watanabe, K., Al-Bassam, S., Miyazaki, Y., Wandless, T.J., Webster, P., and Arnold, D.B. (2012). Networks of polarized actin filaments in the axon initial segment provide a mechanism for sorting axonal and dendritic proteins. Cell Rep. *2*, 1546–1553.

Witte, H., Neukirchen, D., and Bradke, F. (2008). Microtubule stabilization specifies initial neuronal polarization. J. Cell Biol. *180*, 619–632.

Yau, K.W., van Beuningen, S.F., Cunha-Ferreira, I., Cloin, B.M., van Battum, E.Y., Will, L., Schätzle, P., Tas, R.P., van Krugten, J., Katrukha, E.A., et al. (2014). Microtubule minus-end binding protein CAMSAP2 controls axon specification and dendrite development. Neuron *82*, 1058–1073.

Yoshimura, T., Kawano, Y., Arimura, N., Kawabata, S., Kikuchi, A., and Kaibuchi, K. (2005). GSK-3beta regulates phosphorylation of CRMP-2 and neuronal polarity. Cell *120*, 137–149.

Zempel, H., and Mandelkow, E. (2014). Lost after translation: missorting of Tau protein and consequences for Alzheimer disease. Trends Neurosci. *37*, 721–732.